

PAPER • OPEN ACCESS

Detection of alpha heating in JET-ILW DT plasmas by a study of the electron temperature response to ICRH modulation



















To cite this article: P. Mantica *et al* 2024 *Nucl. Fusion* **64** 086001

View the [article online](#) for updates and enhancements.

You may also like

- [Sawtooth pacing with on-axis ICRH modulation in JET-ILW](#)
E. Lerche, M. Lennholm, I.S. Carvalho et al.
- [Ion cyclotron resonance heating for tungsten control in various JET H-mode scenarios](#)
M Goniche, R J Dumont, V Bobkov et al.
- [Predictive multi-channel flux-driven modelling to optimise ICRH tungsten control and fusion performance in JET](#)
F.J. Casson, H. Patten, C. Bourdelle et al.

Detection of alpha heating in JET-ILW DT plasmas by a study of the electron temperature response to ICRH modulation

P. Mantica^{1,*} , F. Auremma² , I. Casiraghi¹, D. Gallart³ , K. Kirov⁴, E. Lerche⁵, A. Salmi⁶ , A. Dal Molin¹ , E. Delabie⁷, J. Eriksson⁸ , J. Garcia⁹ , P. Huynh⁹, P. Jacquet⁴, T. Jonsson¹⁰ , V. Kiptily⁴ , E. Litherland-Smith⁴, C.F. Maggi⁴ , M. Mantsinen^{3,11}, G. Marcer¹², M. Maslov⁴ , S. Menmuir⁴, M. Nocente¹² , E. Peluso^{13,14} , G. Pucella¹⁴ , D. Rigamonti¹ , Z. Stancar⁴ , H. Sun⁴ , G. Szepesi⁴, M. Tardocchi¹, D. Van Eester⁵  and JET Contributors^a

EUROfusion Consortium, JET, Culham Science Centre, Abingdon OX14 3DB, United Kingdom of Great Britain and Northern Ireland

¹ Institute of Plasma Science and Technology, CNR, Milano, Italy

² Consorzio RFX ISTP-CNR, Padova, Italy

³ Barcelona Supercomputing Center, Barcelona, Spain

⁴ UKAEA, Culham Science Centre, Abingdon, United Kingdom of Great Britain and Northern Ireland

⁵ Laboratory for Plasma Physics, ERM/KMS, Brussels, Belgium

⁶ VTT, PO Box 1000, FI-02044 VTT Espoo, Finland

⁷ Oak Ridge National Laboratory, Oak Ridge, TN 37831, United States of America

⁸ Department of Physics and Astronomy, Uppsala University, Uppsala, Sweden

⁹ CEA, IRFM, Saint-Paul-lez-Durance, France

¹⁰ Fusion Plasma Physics, EES, KTH, Stockholm, Sweden

¹¹ ICREA, Barcelona, Spain

¹² University of Milano-Bicocca, Milano, Italy

¹³ University of Rome Tor Vergata, Roma, Italy

¹⁴ ENEA C.R.Frascati, Frascati, Italy

E-mail: paola.mantica@istp.cnr.it

Received 20 February 2024, revised 14 May 2024

Accepted for publication 31 May 2024

Published 18 June 2024



Abstract

In the JET DTE2 campaign a new method was successfully tested to detect the heating of bulk electrons by α -particles, using the dynamic response of the electron temperature T_e to the modulation of ion cyclotron resonance heating (ICRH). A fundamental deuterium (D) ICRH scheme was applied to a tritium-rich hybrid plasma with D-neutral beam injection (NBI).

^a See Maggi *et al* 2024 (<https://doi.org/10.1088/1741-4326/ad3e16>) for JET Contributors.

* Author to whom any correspondence should be addressed.



Original content from this work may be used under the terms of the [Creative Commons Attribution 4.0 licence](https://creativecommons.org/licenses/by/4.0/). Any further distribution of this work must maintain attribution to the author(s) and the title of the work, journal citation and DOI.

The modulation of the ion temperature T_i and of the ICRH accelerated deuterons leads to modulated α -heating with a large delay with respect to other modulated electron heating terms. A significant phase delay of $\sim 40^\circ$ is measured between central T_e and T_i , which can only be explained by α -particle heating. Integrated modelling using different models for ICRH absorption and ICRH/NBI interaction reproduces the effect qualitatively. Best agreement with experiment is obtained with the European Transport Solver/Heating and Current Drive workflow.

Keywords: tokamak, DT plasmas, alpha heating, ICRH modulation

(Some figures may appear in colour only in the online journal)

1. Introduction

Detection of α -particle heating in DT plasmas with fusion gain < 1 is difficult by steady-state power balance analysis, since the α power source is small compared to the external heating and escapes a clear identification due to experimental uncertainties. A new detection method has been attempted in the recent JET DTE2 campaign, based on the dynamic response of the electron temperature T_e to modulated ion cyclotron resonance heating (ICRH) with dominant collisional ion heating. ICRH modulation induces both a modulation in T_i (therefore in α -particles from thermal-thermal fusion reactions) and a modulation in fast D or T ions from neutral beam injection (NBI), depending on the chosen ICRH scheme (therefore a modulation in α -particles from beam-thermal fusion reactions). This modulated electron heating from α -particles has a longer phase delay than other electron heating sources, due to the high energy and long slowing down time of the α -particles, resulting in a delayed T_e response in comparison to the T_i response. Such feature, if observed, may then be clearly identified as due to α -particle heating with the help of detailed integrated modelling to quantify the relative weight of the various modulated electron heating terms at play.

In this paper we present the results of such experiment and the related modelling. Section 2 describes the experimental set-up, section 3 the experimental results for the clearest obtained case, section 4 the modelling of the fast ions and neutron spectra, section 5 the integrated modelling of the plasma response to the modulation, to identify the α contribution. Section 6 summarizes and discusses the results.

2. Experimental set-up

Due to the need of avoiding sawtooth activity for a clearer detection of core temperature modulation, and also to the need of minimizing the level of core ion temperature stiffness to maximize the T_i modulation, the experiments were made on Hybrid scenarios. Specifically, the already developed JET DT Hybrid scenario [1] at 3.4 T, 2.5 MA with 50%–50% D–T mix and ~ 25 MW D + T NBI power and the T-rich Hybrid scenario [2] at 3.86 T, 2.5 MA with 15%–85% D–T mix and ~ 29 MW D NBI power were used, both with ~ 3 –4 MW ICRH power square-wave modulated at 1 Hz with 50% duty-cycle. In the first scenario, ICRH was used in two schemes, a (^3He)-D minority scheme (shot #99639,

$f = 33$ MHz) and a second harmonic D ($\omega = 2 \omega_{\text{cD}}$, with ω_{cD} the cyclotron frequency of the deuterons) majority scheme (shot # 99643, $f = 51$ MHz), whilst in the second scenario a fundamental D ($\omega = \omega_{\text{cD}}$) scheme (shot #99965 and #104523, $f = 28.5$ MHz) was used. The T_e and T_i time evolutions were measured by ECE radiometer [3] and active Charge Exchange spectroscopy using a diagnostic Ne puff [4], the plasma density n_e by high resolution Thomson scattering [5], the radiated power by bolometry [6], the impurity mix was derived by matching both radiation and the measured Z_{eff} . The isotope composition is monitored using sub-divertor spectroscopy measurements [7]. Neutron spectra are measured by diamond detectors [8, 9] and magnetic proton recoil (MPRu) diagnostic upgraded for DTE2 [10].

3. Experimental results

Amongst the 3 ICRH absorption schemes used, best results were obtained in the T-rich Hybrid scenario with the large minority fundamental D ICRH scheme, which maximizes the modulation amplitude of α -particles from non-thermal nuclear reactions. Neutron spectroscopy indicates that the fraction of non-thermal/total fusion reactions is $\sim 85\%$, with an increase of the high energy tails when ICRH is applied. Figure 1 shows the time traces of ICRH, 14 MeV neutrons and plasma total energy for discharge 99965, selected for extensive modelling.

The slow decrease in time of stored energy and neutron rate is due to increasing radiation since ICRH modulation decreases the average ICRH power, reducing its effect of counteracting core W accumulation by boosting turbulent transport and reducing neoclassical inward convection (see e.g. [11]). The obtained neutron (and α) modulation amplitude is $\sim 25\%$ – 35% for an ICRH power modulation $\sim 13\%$ of total power, demonstrating high effectiveness of ICRH in inducing fusion reactions when the D ions are accelerated via fundamental resonance heating [12]. From the total 14 MeV neutron rate (figure 1) by simply multiplying by the energy produced in a fusion reaction (17.6 MeV) one derives that the peak fusion power reached around $t = 7.9$ s is ~ 13 MW, 1/5 of which yields the related peak α -heating of ~ 2.6 MW. The variation of α -power during the considered modulation cycles is ~ 0.5 MW. Figure 2 shows time traces of T_e and T_i at different radii. The number of modulation cycles available for the plasma response analysis is limited. To address this, we

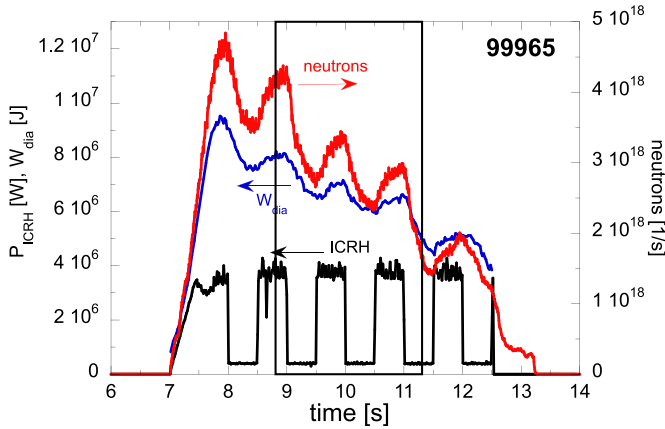


Figure 1. Time traces of ICRH power, neutrons and diamagnetic energy for shot 99965.

are calculating the temperature amplitude and phase profiles by fitting to the temperature time traces the sinusoidal function $A \sin(\omega t - \phi)$ in the 2.5 s time window from 8.85 s to 11.35 s (see figures 1 and 2). The fitting is made independently for each radial time trace (mapped to flux coordinates) after subtracting a linear trend from it. Here, $\omega/2\pi = 1$ Hz is the ICRH modulation frequency, with A and ϕ representing the amplitude and phase, respectively. Notably, a phase increase translates to a time delay increase. The statistical errors in fitting A and ϕ are minimal. The primary source of uncertainty stems from the window selection, given that no two modulation cycles are precisely identical. To quantify this uncertainty, we generated multiple A and ϕ profiles by employing a moving 2 s time window within the 8.85–11.35 s range, and determined error bars based on their standard deviation. Profiles of amplitudes and phases of T_e and T_i modulations are shown in figure 3 as functions of the normalized toroidal radius $\rho_{\text{tor}} = \sqrt{\Phi/\Phi_{\text{edge}}}$ where Φ is the toroidal magnetic flux. The time averaged temperature profiles can be visioned in figure 9 in section 5.

Amplitudes are $\sim 10\%$ of steady-state T profiles, with centrally peaked profiles, as expected. The key result is the large phase delay of $\sim 40^\circ$ of central T_e with respect to T_i . Ions show the typical features of the heat wave propagating from the central ICRH deposition region towards the plasma edge, with phase increasing from the central phase minimum towards the edge until $\rho_{\text{tor}} \sim 0.6$ where edge reflection effects start to affect the phase profile. Electrons show a similar behaviour outside $\rho_{\text{tor}} \sim 0.3$, whilst inside this radius the phase rises sharply towards the centre, departing outside uncertainties from the central ion phase. This delay of $\sim 40^\circ$ of central T_e with respect to T_i modulation is a clear signature that the central T_e modulation is at least in part due to fast ions with high energy and long slowing down times, depositing heat mainly on electrons with large delay. Careful modelling confirmed that such fast ions are the α s and not highly energetic deuterons accelerated by ICRH, as will be discussed later. We note that also the lack of modulation of the few very central T_e channels in the first two cycles (figure 2 lower panel), whilst modulation is visible

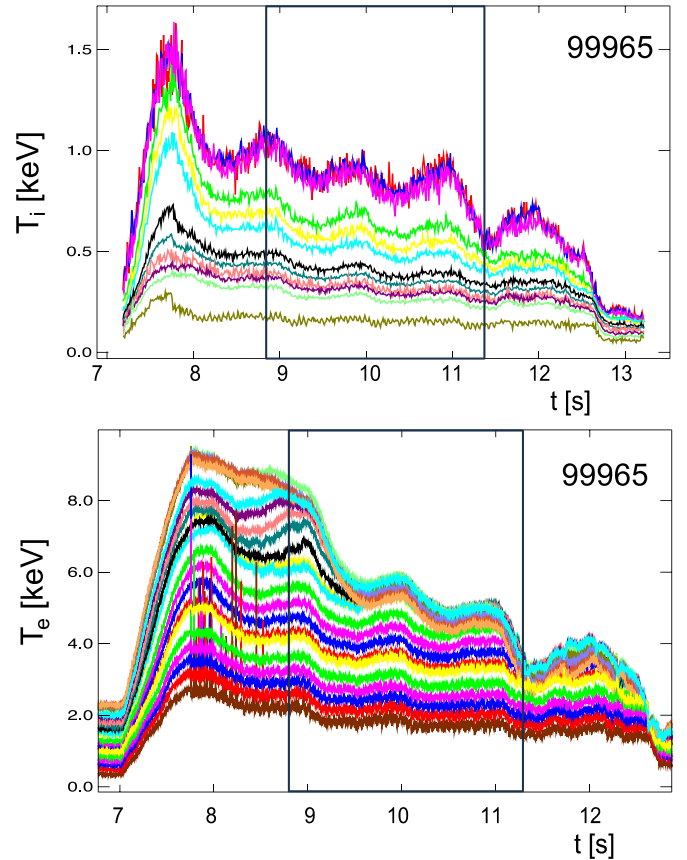


Figure 2. Time traces of T_i and T_e at different radial positions for shot 99965. The rectangle indicates the 2.5 s window used for the amplitude and phase calculation.

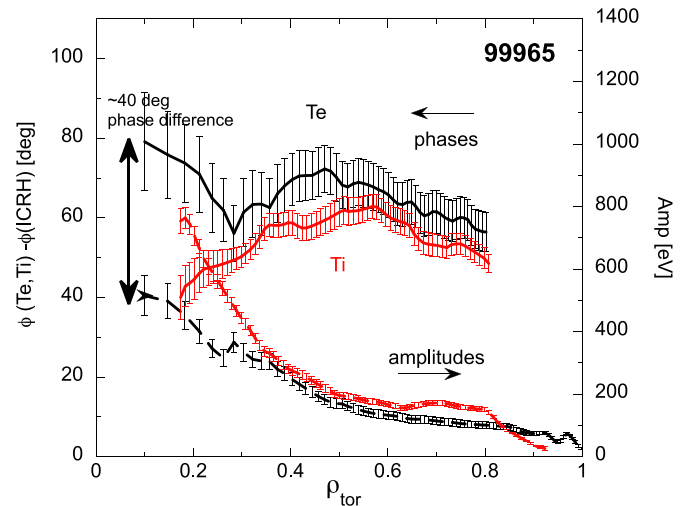


Figure 3. Amplitudes (dashed) and phases with respect to ICRH power (solid) of T_e (black) and T_i (red) for shot 99965, calculated in the 2.5 s window shown in figures 1 and 2.

in T_i and in outer T_e channels, is an indication of a centrally localized source of delayed electron heating, consistent with a high α -particle population in this best performing initial phase of the discharge.

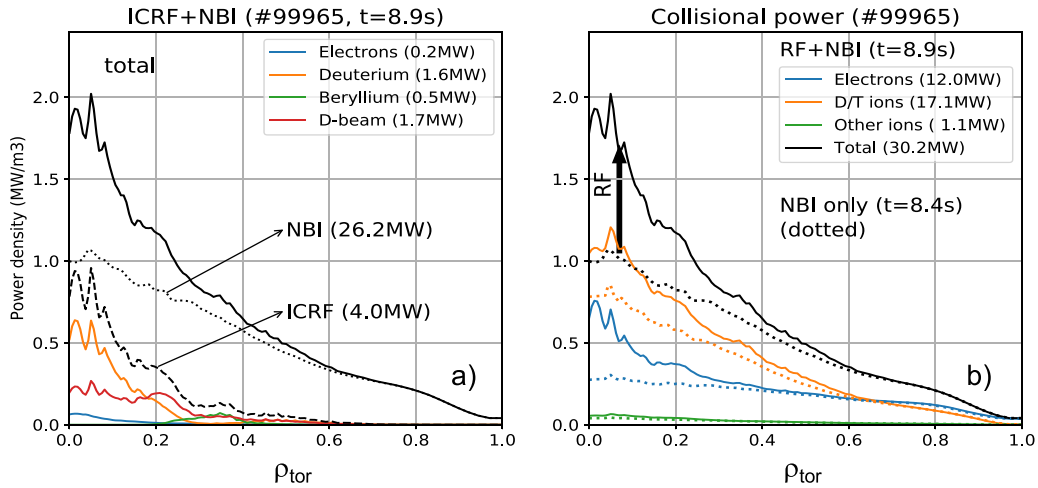


Figure 4. (a) NBI and ICRH power density profiles per species computed by ETS/HCD for discharge 99965 at $t = 8.9$ s; (b) collisional power redistribution to thermal electrons and ions at $t = 8.9$ s, comparing with the case with NBI only at $t = 8.4$ s.

4. ETS simulations of fast ions from external heating and neutron measurements

Modelling of the NBI + ICRH heating depositions has been made using the Heating & Current Drive (H&CD) modules available on the European Transport Solver (ETS) project [13, 14]. This has been run for the two phases of ICRH ON ($\sim t = 8.9$ s) and OFF ($\sim t = 8.4$ s), in a similar way as described in [12] for discharge 99971 which is very similar to 99965 but not modulated. The kinetic profiles were fitted from a combination of the available diagnostics data and the equilibrium was computed with a pressure constrained EFIT simulation. A deuterium concentration of 15% was assumed, measured by high resolution H, D, T Balmer-alpha spectroscopy of a Penning discharge within the neutral gas analysis diagnostic in the JET sub-divertor plenum [7]. An impurity mix of 1% of beryllium and 0.1% of nickel was used. Alpha particle absorption by ICRH was not included. The H&CD workflow was executed as follows: first, the NBI deposition was computed using the ASCOT code [15]. The NBI losses (reionization, shine-through, etc) are taken into account and only the remaining ‘slowing-down’ power ($P_{\text{NBI}} = 26.2$ MW) is retained in the next steps. Then, the ICRH power absorption profiles for all species were computed using the 2D full wave CYRANO code [16], assuming $P_{\text{ICRH}} = 4$ MW (ICRH ON) or $P_{\text{ICRH}} = 0.4$ MW (ICRH OFF) is absorbed in the plasma. The obtained RF-fields and power absorption profiles are used as input for the Fokker–Planck code FOPLA [17], which computes the 1D distribution functions of all the ions in the plasma (including self-collisions) and the converged collisional power repartition. The set of radial distributions functions obtained for the bulk D and T ions and for the D-beam ions are then used to compute the D–T fusion reaction profiles (neutrons and α ’s) with the combined effect of ICRH and NBI heating, using the FUSREAC module, included in the ETS/HCD workflow. The results of the simulations for discharge 99965 with ICRH ON and OFF are shown in figure 4, where one can see that the ICRH power density profile is much narrower than NBI one and mainly deposited on D_{bulk} and D_{NBI} , which are both

accelerated by ICRH to form tails with 50–200 keV, as shown in figure 5. This range of energies for the D tails is also confirmed by the Neutral Particle Analyzer spectra, as shown for shot #99965 in figure 4(a) of [12]. These tails boost the fusion reactions, inducing the large modulation of neutrons and α -particles, as shown in figure 6. ETS modelling confirms that thermal reactions are $\sim 15\%$ of the total. It is important to note that, although ETS cannot handle dynamic simulations, the comparison of fusion power density profiles obtained using the ETS D populations with and without ICRH provides an estimate of the expected P_{α} variation ~ 0.16 MW m^{-3} , localized inside $\rho_{\text{tor}} \sim 0.35$, i.e. within the ICRH deposition region. This is actually in good agreement with the radius where the T_e modulation phase starts departing from the T_i phase in figure 3. Given the range of energy 50–200 keV calculated by ETS for the D population, with slowing down times < 40 ms, corresponding to $< 14^\circ$ for a 1 Hz modulation, we can conclude that the ICRH accelerated D fast ions are not responsible for the central T_e delay of $\sim 40^\circ$ observed in the experiment. This leaves α -heating as the only possible mechanism causing the central T_e delay. In fact α s have a slowing down time ~ 350 ms in the central region, corresponding to a phasing at 1 Hz of $\sim 120^\circ$, and so they are the only possible source of electron heating that combined with the NBI + ICRH faster sources can lead to the observed T_e delay of 40° . We note also that the amount of variation of P_{α} (figure 6(b)) is a factor 1/2–1/3 of the variation of P_e from NBI + RF (figure 6(c)), which, given their phasing, yields the correct phasing of the summed P_e terms to justify the observed T_e delay of $\sim 40^\circ$. We conclude that ETS, in spite of not allowing a time dependent simulation of the modulation, yields predictions in very good agreement with the experimental observations for what concerns the magnitude of the T_e delay and its spatial localization.

The ETS simulations have been used as input to the GENESIS code [18] to calculate the neutron production and compare with neutron spectroscopy data. The GENESIS code is a Monte Carlo code that simulates the energy spectrum of neutron and γ -ray radiation from the plasma starting from the distribution functions of the reactants, as obtained by

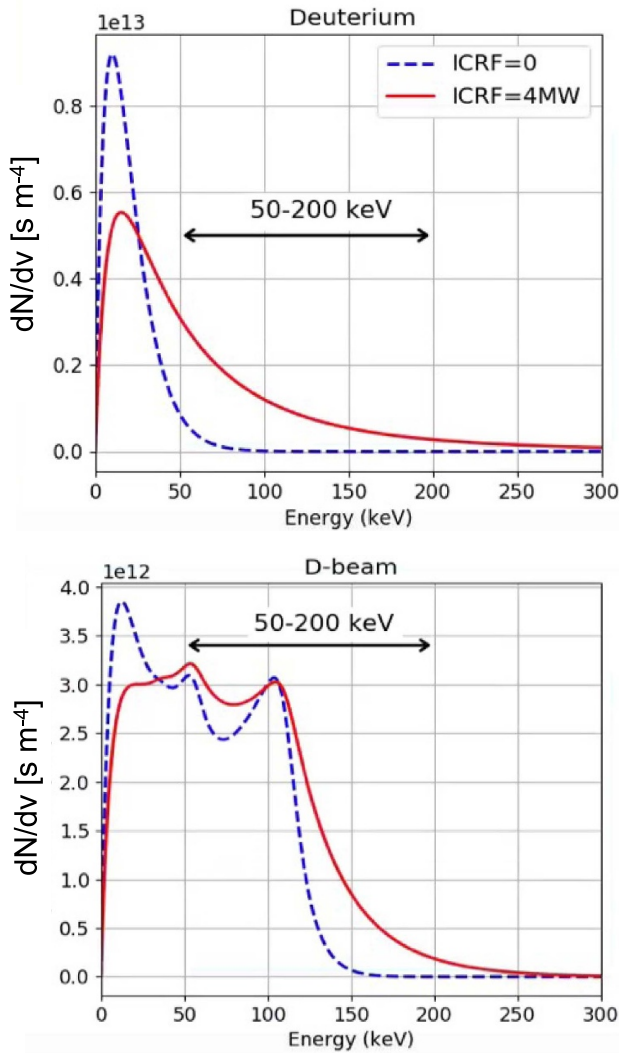


Figure 5. Particle density distributions in velocity space of bulk D and NBI D as functions of energy at $\rho_{tor} = 0.1$ from ETS simulations of #99965 for ICRH ON (ICRF = 4 MW) and OFF (ICRF = 0 MW). $dN/dv = 4\pi v^2 F_0(v)$ for an isotropic particle distribution function F_0 , with v the particle velocity modulus.

modelling codes such as ETS-FoPla, and the measured plasma profiles. The code can calculate the emission spectrum emitted along the line of sight of the main JET neutron and gamma-ray spectrometers, for a direct comparison with measured data and once the response function of the detector is taken into account. The MPRu spectrometer is the state-of-the-art instrument at JET for the 14 MeV neutron spectrometer measurements. It is based on the momentum separation via magnetic field of the elastically scattered protons on a thin converter foil (CH₂). The measurement of the proton dispersion on an array of scintillators is then related to the distribution of the primary neutron energy spectrum. JET is also equipped with a set of single crystal diamond detectors. Unlike the MPRu that is bulky and heavy, single crystal diamond detectors are very compact in size and can be installed on different line of sight providing 14 MeV neutron spectroscopy measurements with unprecedented energy resolution (about 1%) [9]. Here the neutron detection relies on gathering the electro-hole pairs

generated through the slowing down of charged particles resulting from interactions between neutrons and carbon nuclei. Although different reaction channels can occur between the neutrons and the carbon nuclei, the best candidate for 14 MeV neutron spectroscopy measurements is the $n-\alpha$ reaction $^{12}C(n,\alpha)^9Be$ which has a negative Q -value of -5.7 MeV. The reaction leads to a well-defined peak in the measured neutron spectrum which is centred at $E_{dep} = E_n - 5.7$ MeV. The peak provides a univocal relation between the measured deposited energy and the incoming neutron energy. Figure 7 shows with symbols the experimental neutron spectra from the vertical diamond detector for the ICRH ON and OFF phases. One can notice the increase of the high energy tails due to ICRH. The lines in figure 7 indicate the contributions to the neutron spectra due to the D_{bulk} and D_{NBI} populations, provided by the code GENESIS. The GENESIS simulations are in good agreement with the measured spectra for both phases. A sensitivity test on the D fraction has shown that best match is obtained with the measured 15% D concentration.

Tomographic reconstructions of the neutron emission were performed using the data collected by the JET neutron camera. The poloidally averaged neutron emission profiles were then computed as a function of ρ_{tor} , removing the linear slow trend. The difference in the emission profiles between two adjacent ICRH ON and OFF intervals is shown in figure 8 and compared with the variations predicted by ETS (figure 6(b)) and also TRANSP and JINTRAC discussed later. All variations are normalized to 1 to compare profiles. The experimental mean emission profile is overplotted. The uncertainties in the 1D radial emission profile are calculated by factoring in a 10% margin of error on the intensities derived from the 2D tomographic reconstruction of the poloidal neutron emission profile. This margin of error in the tomography considers a 10% deviation from the nominal detection efficiency of the individual detectors within the neutron camera. From figure 8 we observe that the agreement is reasonable for ETS and JINTRAC, whilst the TRANSP profiles are definitely too broad.

5. Integrated modelling with and without α -heating

Unfortunately, ETS/HCD cannot handle dynamic simulations, therefore integrated modelling of the 99965 modulation had to be made with other frameworks, which have a less sophisticated treatment of heating deposition to the thermal and suprathermal populations, and of the ICRH-NBI interaction. Presently integrated modelling of 99965 has been made with TRANSP/NUBEAM [19] and JINTRAC/PION [20, 21] and results compared to gain confidence in the results. Issues in the models have been identified and an optimization of these tools for the case considered has been attempted.

5.1. TRANSP modelling results

In this section we describe the results of TRANSP predictive simulations of discharge 99965, although it is known that TRANSP does not accurately compute the heating, fast particles and fusion yield in discharges employing the

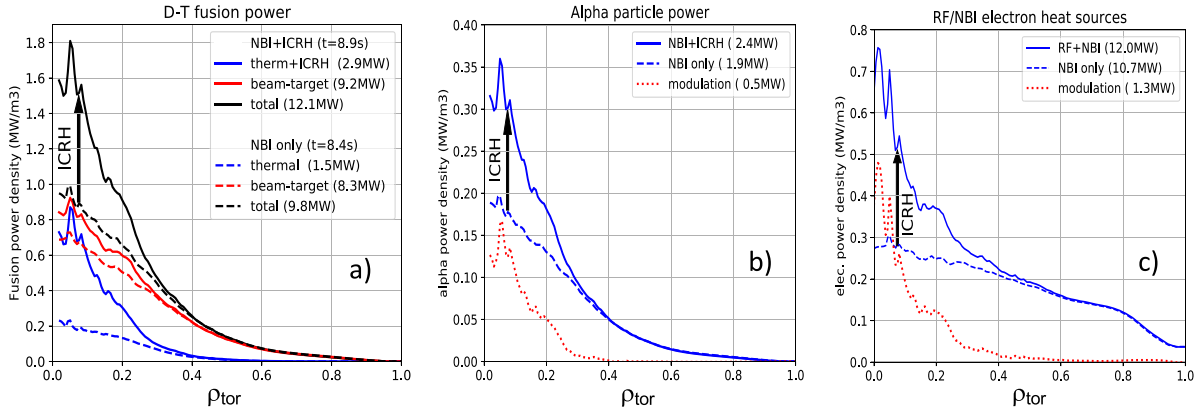


Figure 6. (a) Profiles of fusion power components from ETS simulations of #99965 for ICRH ON and OFF; (b) profiles of α -electron heating and (c) of RF + NBI electron heating and their variation with ICRH ON and OFF according to ETS.

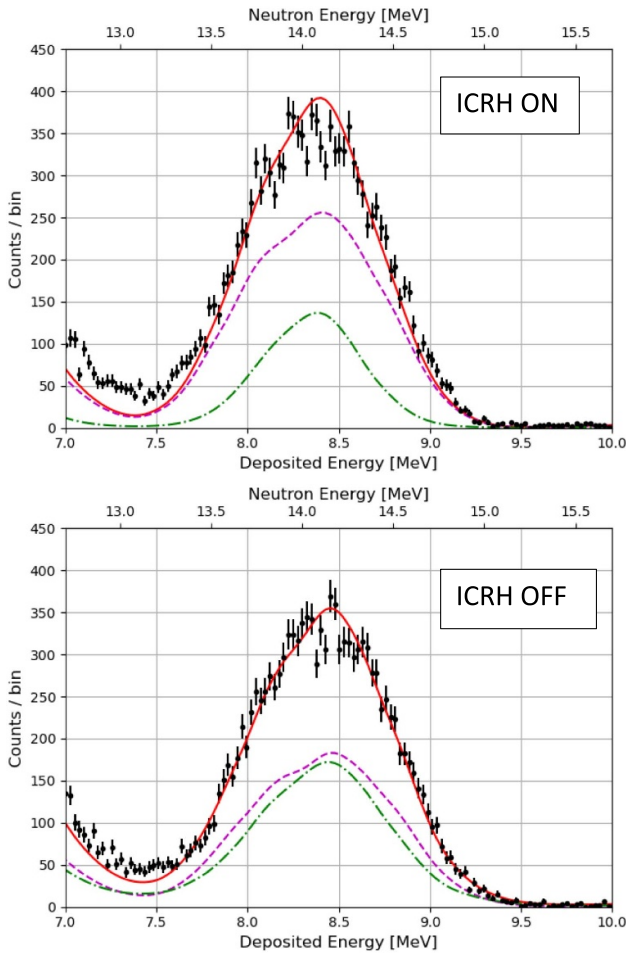


Figure 7. Experimental neutron spectra for #99965 from vertical diamond detector (symbols) for ICRH ON ($t = 8.8$ – 9 s) and OFF ($t = 8.3$ – 8.5 s) phases compared with total neutrons calculated by GENESIS from ETS simulations (—). Neutron components produced by D_{bulk} (---) and D_{beam} (---) are also shown. The explanation of the difference between neutron energy and deposited energy is provided in the main text.

fundamental RF heating of a large minority, as discussed in detail in [22]. ICRH heating in TRANSP is modelled by the TORIC code [23] coupled to the time dependent FPP code for

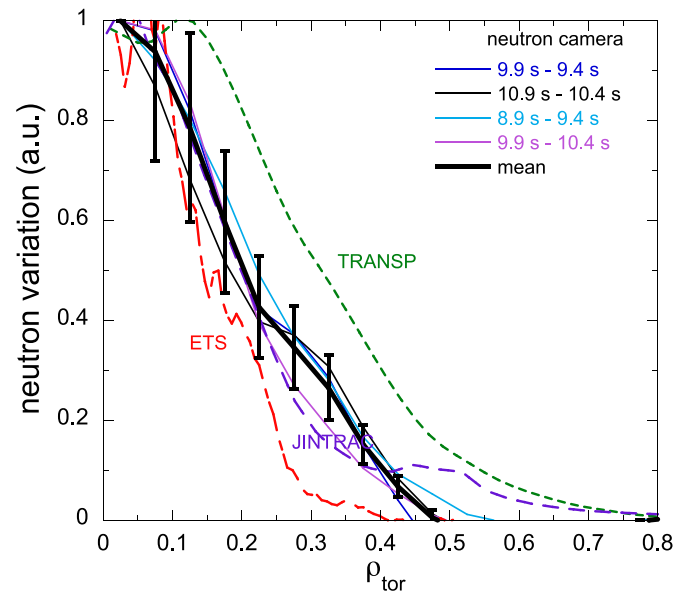


Figure 8. Radial profiles of neutron emission variation (normalized to 1) between ICRH ON and OFF for #99965, obtained by tomographic reconstruction from the neutron camera data and predicted by ETS, TRANSP and JINTRAC. The experimental profiles refer to 4 time intervals and their mean value (black thick line).

absorption by minorities and by means of a RF kick operator in the NUBEAM Monte-Carlo code for absorption by fast NBI ions and alphas. As shown in figure 5 by ETS/HCD, in this fundamental D (with $D \sim 15\%$) heating scenario, the Maxwellian distribution of the bulk D ions is accelerated by the RF interaction and forms an energetic tail, and in addition there is a synergy effect between the RF waves and the fast NBI deuteron population. Both D populations contribute to fusion reactions. TRANSP can describe the NBI-ICRH interaction with the quasi-linear RF kick operator, but it cannot fully model the absorption of RF power on bulk thermal species and requires defining a dedicated fast RF minority species. However, on one hand D_{minority} is not taken into account for fusion reactions, on the other hand the D tails produced by ICRH from D_{bulk} are not calculated, and absorption on

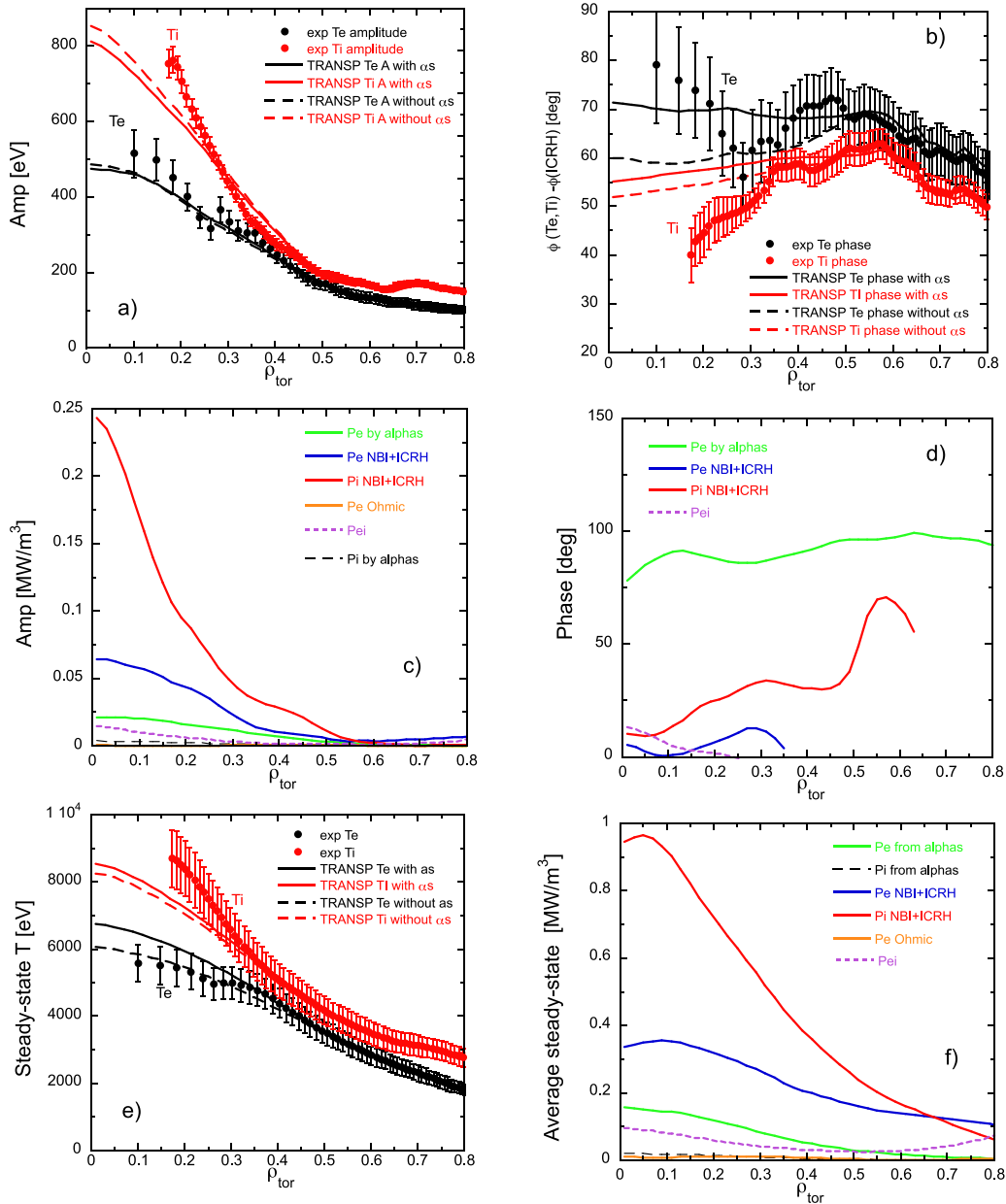


Figure 9. For shot #99965: radial profiles of modulation (a) amplitudes, (b) phases and (e) averaged steady-state of T_e and T_i (experimental data vs TRANSP predictions, in the same time window as in figure 3). Radial profiles of modulation (c) amplitudes, (d) phases and (f) averaged steady-state of power densities. In (a), (b) and (e) runs with and without α s are compared.

D_{bulk} results in a direct ion heating term whilst keeping a Maxwellian distribution. This evidently is inappropriate for describing the 99965 scenario, and even more so when the dynamic modelling and heating delay is key to the explanation of results. However, owing to the good neutron rate predictability of TRANSP, an effort has been made to use the code by separating D ions into bulk D ions and minorities D and using NUBEAM D NBI as in experiment. In order to best capture RF wave physics and fusion rates by thermal and beam-target reactions, optimised settings were found by using 86% T + 7% D_{bulk} , NUBEAM with all D beams as in experiment, and TORIC with 7% D_{minority} . This setup was optimised by means of TRANSP scans and has been found to be the best compromise to account for both bulk D and fast D species dynamics as well as the two kinds of interactions D ions are

subject to: collisions and fundamental ICRH resonance. The simulations were performed using a simplified transport model with non-evolving heat diffusivities χ_i and χ_e approximating the power balance diffusivities. Presently, all attempts to use quasi-linear physics-based transport models do not yield clear results due to the noise introduced by these models. As boundary conditions for T_e and T_i the experimental measurements at $\rho_{\text{tor}} = 0.5$ were used, to avoid simulating the region where edge effects are important. Simulations were run both including and not including α -particle heating, to isolate clearly the effect of α s. Amplitudes and phases of the modulation cycles as well as the time averaged steady-state profiles, were calculated with same technique used for the experimental data.

The results are shown in figure 9. Figures 9(c) and (d) show amplitude and phases of the modulation of the various

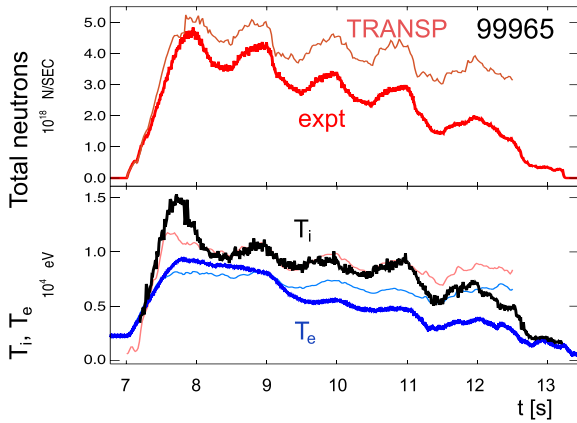


Figure 10. Comparison of experimental (thick lines) and TRANSP (thin lines) central T_e and T_i and total neutrons vs time. T_i from TRANSP is plotted in red to better distinguish it from the black experimental data.

heating terms, and figure 9(f) shows their time averaged profiles. From figure 9(d) it is important to note that the phasing of the external power is very low whilst the phasing of α s is long (consistent with the short slowing down time of the fast deuterons and the long one of α s, as discussed for ETS results). This confirms that the only possible explanation for the large T_e central delay is the α -heating. However, compared to ETS, the radial profile of the amplitude of the P_α modulation is broader, extending to $\rho_{\text{tor}} \sim 0.6$, and the peak central value is less than half the peak value of the external electron power (figure 9(c) vs figure 6(b), directly compared in absolute values in figure 12, and in terms of normalized neutron variation for peaking comparison in figure 8). This results in the effect of α -heating on the T_e phasing being visible in the whole simulated region rather than localized inside $\rho_{\text{tor}} \sim 0.3$, and with a central delay much smaller than in the experiment (figure 9(b)). Figure 10 shows the comparison of central waveforms of neutrons and temperatures between experiment and TRANSP simulations. We conclude that TRANSP provides a qualitative reproduction of the features seen in the temperature modulations, with reasonable match of the amplitudes but an underestimate of the delay on T_e . This seems due to a too broad α -particle profile, linked to non-correct prediction of the profile of the ICRH + NBI fast deuterons. Nevertheless, this modelling shows that indeed the only mechanism that can produce the measured T_e delay is the α -heating.

5.2. JINTRAC modelling results

JINTRAC/PION + PENCIL runs were performed to try and improve over TRANSP integrated modelling results. The PION code [21] solves the power absorption and the velocity distribution function of resonant particles in a self-consistent way. The Fokker–Planck solver in PION does not assume steady-state conditions and, therefore, it is able to capture plasma transitions. Furthermore, PION takes into account finite orbit width (FOW) effects which are relevant when high energy resonant particles are produced, effectively extending the electron collisional heating to larger flux surfaces.

The PENCIL code [24] computes the NBI source which is used by PION's Fokker Planck solver. Based on this, PION is capable of reproducing the ICRH + NBI synergy by solving the full distribution of the resonant particles, in this case for D (it does not make a difference between bulk and fast/NBI, everything is accounted for in its distribution function).

JINTRAC integrated modelling was performed with the same input initial profiles and equilibria as for the TRANSP simulations, then evolved self-consistently solving for T_e , T_i , and J whilst keeping the n_e and rotation profiles fixed to the experimental ones. The same simplified transport model was used as in TRANSP simulations, with non-evolving heat diffusivities χ_i and χ_e approximating the power balance diffusivities. As boundary conditions for T_e and T_i the experimental measurements at $\rho_{\text{tor}} = 0.5$ were used, as in the TRANSP runs. Simulations were run both including and not including α -particle heating, to isolate the effect of α s. The results were then analysed to extract the 1 Hz modulation in the same time window 8.85–10.35 s. Figures 11(c)–(f) show amplitudes, phases and time-averaged profiles for the modulation of the various heating terms. Here again in figure 11(d) the phasing of the external power is low compared to the phasing of α s, confirming that the only possible explanation of the large T_e central delay is the α -heating. The width of the P_α modulation amplitude (figure 11(c) vs figure 6(b), directly compared in absolute values in figure 12, and in terms of normalized neutron variation for peaking comparison in figure 8) is similar to ETS, but in fact its central value is similar to TRANSP and a factor 3 lower than ETS. This is much lower than the P_e amplitude from NBI + ICRH, so the effect on T_e amplitude and phase is visible in figures 11(a) and (b), but the 10° delay due to α s is much smaller than the 40° measured. We also note in figure 11(c) that the P_i amplitude from NBI + ICRH is very broad and with larger phasing than P_e , so that the T_i phasing is flat in the central region and higher than the T_e phasing, at variance with experiment where the T_i has a clear propagating character, suggesting a much narrower P_i modulation profile. Figure 13 shows the experimental neutrons and central temperatures compared with the JINTRAC simulation. We conclude that the JINTRAC/PION simulations, although clearly indicating that α -heating is the only possible cause for the large T_e delay, have issues in reproducing correctly the measured phasing, as was the case for TRANSP simulations. Besides underestimating the T_e delay (as in TRANSP), there is also an issue with the large T_i phasing (at variance with experiment), whose origin is difficult to understand. For this reason, further investigations were made to assess the origin of the discrepancy between experimental and modelling results on the phase of ion and electron temperatures. Several possibilities were studied, such as FOW effects and fast ion losses in PION, however their impact has been found small in these simulations and is not the cause for the P_i amplitude broadening. In our investigation, interpretative simulations were conducted for ICRH and NBI heating, each modelled independently. Fourier analysis of the simulations reveals distinct characteristics for these heating mechanisms. The Fourier analysis of simulations focused solely on ICRH demonstrates a clear modulation at 1 Hz. Notably, the ion–electron collisional power exhibits a

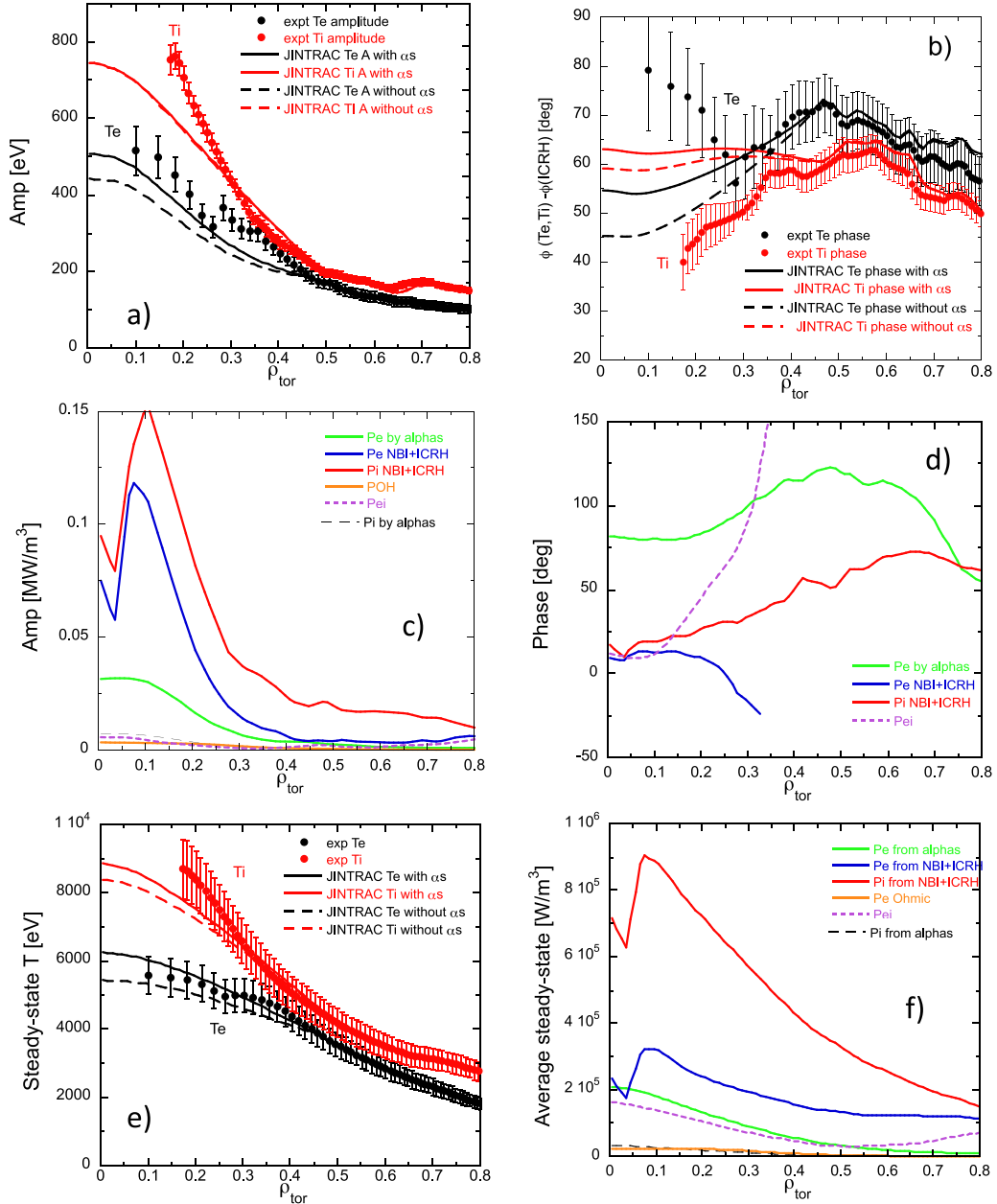


Figure 11. For shot #99965: radial profiles of modulation (a) amplitudes, (b) phases and (e) averaged steady-state of T_e and T_i (experimental data vs JINTRAC predictions, in the same time window as in figure 3). Radial profiles of modulation (c) amplitudes, (d) phases and (f) averaged steady-state of power densities. In (a), (b) and (e) runs with and without α s are compared.

higher phase compared to ion–ion collisional power, aligning with expectations. In contrast, simulations utilizing only the NBI source from PENCIL show a significant and broad amplitude at 1 Hz, which causes the P_i amplitude broadening. Furthermore, ion–ion collisional power displays a larger phase compared to ion–electron collisional power. When considering both ICRH and NBI, the ion–electron collisional power phasing, accounting also for ICRH + NBI synergy, is lower than that of ion–ion collisional power phasing. This results in a larger T_i phasing compared to T_e , i.e. a delayed T_i signal as opposed to what is observed experimentally. To further investigate the impact of NBI on ion–ion collisional power, a

Fourier correction was applied to the NBI signal during the interpretative simulation without compromising the total NBI power. This correction successfully recovered the expected collisional power phasing values, indicating a delayed central ion–electron collisional power compared to ion–ion collisional power. Nevertheless, as the simulations presented in this paper are predictive, the Fourier correction tested in interpretative simulations could not be applied to assess its impact on modelled temperatures. Therefore, to enhance agreement with experimental results, future efforts could explore coupling more sophisticated NBI codes, such as ASCOT, with PION.

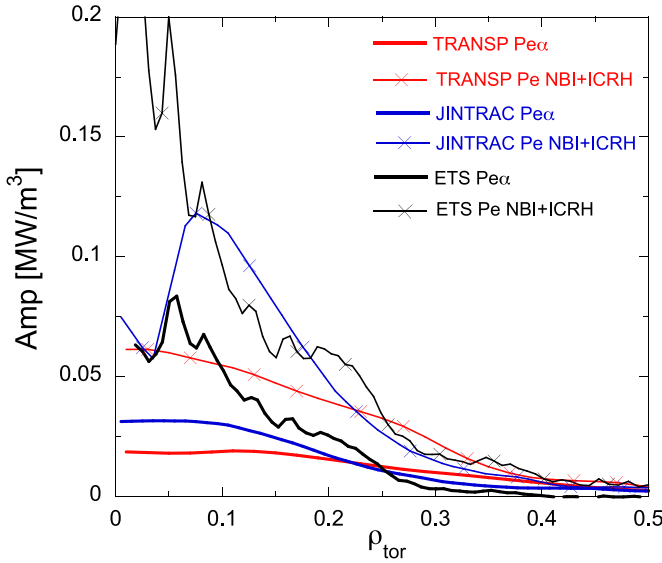


Figure 12. Profiles of amplitudes of modulation of P_α and P_e from NBI + ICRH from ETS, TRANSP and JINTRAC for #99965.

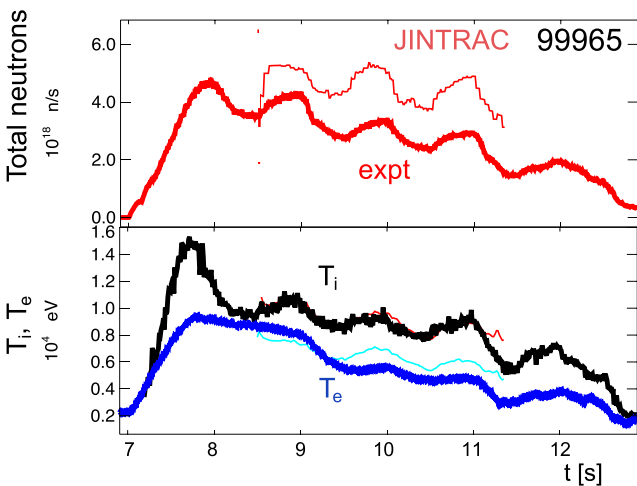


Figure 13. Comparison of experimental (thick lines) and JINTRAC (thin lines) central T_e and T_i and total neutrons vs time. T_i from JINTRAC is plotted in red to better distinguish it from the black experimental data.

6. Conclusions

Dynamic detection of α -particle electron heating was possible in JET DTE2 by using 4 MW modulated ICRH at 1 Hz with the fundamental D heating scheme in the JET T-rich Hybrid scenario at 3.86 T, 2.5 MA with 15%–85% D–T mix and ~ 29 MW D NBI power. Experimentally, a $\sim 40^\circ$ phase delay of central T_e with respect to T_i was observed, which cannot be explained by high energy tails of NBI + ICRH fast deuterons and constitutes evidence for electron α -heating. We underline that extraction of the electron α -heating is difficult in JET DT plasmas as the α -population is still quite low and the electron α -heating term has to compete with other larger electron heating terms. Therefore an analysis based on steady-state power balance is not able to isolate the electron α -heating

outside uncertainties. The use of dynamic methods adds the time information, which is a precious ingredient given the long slowing down time of alphas. Dynamic methods have then proven successful in JET DT plasmas where α -production has been maximized by suprathreshold fusion reactions. An alternative dynamic method to the modulation presented here is the afterglow experiment described in [25], which also showed a clear delay in T_e fall after the complete switch-off of the external heating. This method is however more perturbative than the smaller modulation of the ICRH power described here, which maintains a good confinement plasma with no density perturbation, apart from the slower decreasing trend due to W accumulation. We remark that these experimental results are the first ever evidence of α -heating obtained by modulation techniques.

On the modelling side, ETS-HCD simulations for the ICRH ON and OFF phase are found in good match with the experimental observation, both in terms of magnitude of the T_e delay and its spatial localization inside $\rho_{\text{tor}} \sim 0.3$. TRANSP and JINTRAC integrated modelling instead predict a significantly smaller central α -heating and do not reproduce the T_e phase profile observed experimentally. These dynamic experiments provide constraining evidence against which present codes can be tested and improved in view of their application to ITER and beyond.

Acknowledgments

This work was carried out within the framework of the EUROfusion Consortium, funded by the European Union via the Euratom Research and Training Programme (Grant Agreement No. 101052200—EUROfusion). Views and opinions expressed are, however, those of the authors only and do not necessarily reflect those of the European Union or the European Commission. Neither the European Union nor the European Commission can be held responsible for them.

The BSC part of this work are grateful for the support received from the Departament de Recerca i Universitats de la Generalitat de Catalunya via the Research Group Fusion Group with code: 2021 SGR 00908.

The authors are grateful to Dr L. -G. Eriksson for his support and discussions.

ORCID iDs

P. Mantica <https://orcid.org/0000-0001-5939-5244>
 F. Auriemma <https://orcid.org/0000-0002-1043-1563>
 D. Gallart <https://orcid.org/0000-0003-1663-3550>
 A. Salmi <https://orcid.org/0000-0002-3306-6335>
 A. Dal Molin <https://orcid.org/0000-0003-0471-1718>
 J. Eriksson <https://orcid.org/0000-0002-0892-3358>
 J. Garcia <https://orcid.org/0000-0003-0900-5564>
 T. Jonsson <https://orcid.org/0000-0002-7142-7103>
 V. Kiptily <https://orcid.org/0000-0002-6191-7280>
 C.F. Maggi <https://orcid.org/0000-0001-7208-2613>
 M. Maslov <https://orcid.org/0000-0001-8392-4644>

M. Nocente  <https://orcid.org/0000-0003-0170-5275>
 E. Peluso  <https://orcid.org/0000-0002-6829-2180>
 G. Pucella  <https://orcid.org/0000-0002-9923-2770>
 D. Rigamonti  <https://orcid.org/0000-0003-0183-0965>
 Z. Stancar  <https://orcid.org/0000-0002-9608-280X>
 H. Sun  <https://orcid.org/0000-0003-0880-0013>
 D. Van Eester  <https://orcid.org/0000-0002-4284-3992>

References

- [1] Hobirk J. *et al* 2023 *Nucl. Fusion* **63** 112001
- [2] Maslov M. *et al* 2023 *Nucl. Fusion* **63** 112002
- [3] Luna E.D.L., Sánchez J., Tribaldos V., Conway G., Suttrop W., Fessey J., Prentice R., Gowers C. and Chareau J.M. (JET-EFDA Contributors) 2004 *Rev. Sci. Instrum.* **75** 3831
- [4] Hawkes N.C., Delabie E., Menmuir S., Giroud C., Meigs A.G., Conway N.J., Biewer T.M. and Hillis D.L. 2018 *Rev. Sci. Instrum.* **89** 10D113
- [5] Frassinetti L., Beurskens M.N.A., Scannell R., Osborne T.H., Flanagan J., Kempenaars M., Maslov M., Pasqualotto R. and Walsh M. 2012 *Rev. Sci. Instrum.* **83** 013506
- [6] Huber A. *et al* 2007 *Fusion Eng. Des.* **82** 1327
- [7] Vartanian S. *et al* 2021 *Fusion Eng. Des.* **170** 112511
- [8] Rigamonti D. *et al* 2018 *Meas. Sci. Technol.* **29** 045502
- [9] Rigamonti D. *et al* 2024 *Nucl. Fusion* **64** 016016
- [10] Sunden E. *et al* 2009 *NIM* **A610** 682
- [11] Goniche M. *et al* 2017 *Plasma Phys. Control. Fusion* **59** 055001
- [12] Lerche E. *et al* 2023 *24th Topical Conf. on Radio-Frequency Power in Plasmas, AIP Conf. Proc.* vol 2984 p 030005
- [13] Kalupin D. *et al* 2013 *Nucl. Fusion* **53** 123007
- [14] Strand P. *et al* 2018 *27th IAEA Fusion Energy Conf. (Proc. Int. Conf. Gandhinagar, India, 2018, CN-258, #451, TH/P6-14) (Vienna)*
- [15] Hirvijoki E., Asunta O., Koskela T., Kurki-Suonio T., Miettunen J., Sipilä S., Snicker A. and Äkäslompolo S. 2014 *Comput. Phys. Commun.* **185** 1310
- [16] Lamalle P. 1994 *PhD Thesis LPP-ERM/KMS, Report 101* Université de Mons
- [17] Van Eester D. and Lerche E. 2011 *Plasma Phys. Control. Fusion* **53** 092001
- [18] Tardocchi M. *et al* 2011 *Phys. Rev. Lett.* **107** 205002
- [19] Budny R.V. *et al* 1995 Simulations of alpha parameters in a TFTR DT supershot with high fusion power *Nucl. Fusion* **35** 1497
- [20] Romanelli M. *et al* 2014 JINTRAC: a system of codes for integrated simulation of tokamak scenarios *Plasma Fusion Res.* **9** 3403023
- [21] Eriksson L.-G., Hellsten T. and Willen U. 1993 Comparison of time dependent simulations with experiments in ion cyclotron heated plasmas *Nucl. Fusion* **33** 1037
- [22] Stancar Ž. *et al* 2023 *Nucl. Fusion* **63** 126058
- [23] Brambilla M. 1999 Numerical simulation of ion cyclotron waves in tokamak plasmas *Plasma Phys. Control. Fusion* **41** 1–34
- [24] Challis C., Cordey J.G., Hamnén H., Stubberfield P.M., Christiansen J.P., Lazzaro E., Muir D.G., Stork D. and Thompson E. 1989 *Nucl. Fusion* **29** 563
- [25] Kiptily V.G. *et al* 2023 *Phys. Rev. Lett.* **131** 075101